Inorganic Chemistry

Article

pubs.acs.org/IC

Synthesis of Copper–Antimony-Sulfide Nanocrystals for Solution-Processed Solar Cells

Satoshi Suehiro,[†] Keisuke Horita,[†] Masayoshi Yuasa,[‡] Tooru Tanaka,[§] Katsuhiko Fujita,[∥] Yoichi Ishiwata,[⊥] Kengo Shimanoe,[‡] and Tetsuya Kida*[,#]

[†]Department of Molecular and Material Sciences, Interdisciplinary Graduate School of Engineering Sciences, [‡]Department of Energy and Material Sciences, and [∥]Institute for Materials Chemistry and Engineering, Kyushu University, Kasuga Koen 6-1, Fukuoka 816-8580, Japan

[§]Department of Electrical and Electronic Engineering and [⊥]Department of Physics, Saga University, Honjo 1, Saga 849-8502, Japan

[#]Department of Applied Chemistry and Biochemistry, Kumamoto University, Kurokami 2-39-1, Kumamoto 860-8555, Japan

ABSTRACT: The p-type nanocrystals (NCs) of copper-based chalcogenides, such as $CuInSe_2$ and Cu_2ZnSnS_4, have attracted increasing attention in photovoltaic applications due to their potential to produce cheap solution-processed solar cells. Herein, we report the synthesis of copper–antimony-sulfide (CAS) NCs with different crystal phases including $CuSbS_2$, Cu_3SbS_4, and $Cu_{12}Sb_4S_{13}$. In addition, their morphology, crystal phase, and optical properties were characterized using transmission electron microscopy, X-ray diffractometry, UV–vis–near-IR spectroscopy, and photoemission yield spectroscopy. The morphology, crystal phase, and electronic structure were significantly dependent on the chemical composition in the CAS system. Devices were fabricated using particulate films consisting of CAS NCs prepared by spin coating without a high-temperature treatment. The CAS NC-based devices exhibited a diode-like current–voltage characteristic when coupled with an n-type CdS layer. In particular, the $CuSbS_2$ NC devices exhibited photovoltaic responses under simulated sunlight, demonstrating its applicability for use in solution-processed solar cells.

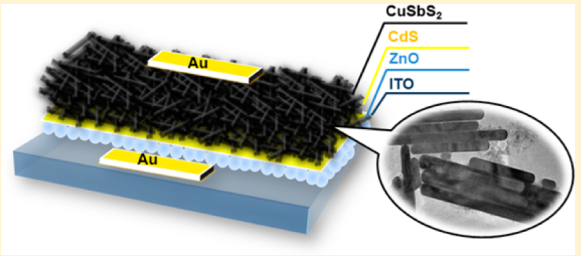

INTRODUCTION

Thin films based on CdTe[1] and $Cu(In_{1-x}Ga_x)Se$[2] have attracted much attention as excellent absorbers for low-cost solar cells. These solar cells have recently achieved high efficiencies of 15–20%. However, the scarcity of In, Ga, and Te limits their sustainable production. Therefore, alternative materials that are earth-abundant and nontoxic must be explored. Sulfide materials, such as Cu_2ZnSnS_4,[3] Cu_2SnS_3,[4] Fe_2S,[5] and SnS,[6] have been extensively studied for several years.

Recently, some studies have reported promising features of $CuSbS_2$ and $CuBiS_2$ as new candidates for p-type absorber materials based on first-principles calculations using density functional theory.[7,8] The results from the calculations indicated that $CuSbS_2$ has an optical band gap of 1.6–1.8 eV and a strong light absorption coefficient ($\alpha > 1 \times 10^4$ cm^{-1}), which are comparable to those for $CuInS_2$ and Cu_2ZnSnS_4. The copper–antimony-sulfide (CAS) systems exist as multiple phases including $CuSbS_2$ (chalcostibite), Cu_3SbS_4 (skinnerite), Cu_3SbS_4 (fematinite), and $C_{12}Sb_4S_{13}$ (tetrahedrite). All of these materials have similar band gaps and high absorption coefficients.

However, only a few studies utilizing CAS materials for solar cells have been reported. Lazcano et al. reported a photovoltaic (PV) device using a $CuSbS_2$ film prepared by wet chemical deposition.[9] In this study, an open-circuit voltage (V_{oc}) of 345 mV and short-circuit current (J_{sc}) of 0.18 mA/cm^2 were observed under light irradiation (1 kW/m^2) using a device structure consisting of glass/FTO/CdS:In/Sb_2S_3/$CuSbS_2$ (FTO = fluorine-doped tin oxide). Recently, Yang et al. reported a PV device consisting of a glass/FTO/$CuSbS_2$/ZnO/ZnO:Al/Au structure with a $CuSbS_2$ layer that was fabricated using a hydrazine-based solution process.[10] This device exhibited a light conversion efficiency of 0.5%.

In general, the absorber layers in solar cells are prepared using vacuum processes. In an effort to develop more cost-effective processes, an alternative route that deposits the absorber layers by coating with a dispersion of semiconductor nanocrystals (NCs) has recently been developed. This route may allow for large-scale production of thin films based on a roll-to-roll method. Solution-processed semiconductor NC-based solar cells represent an alternative printed device to organic solar cells. Currently, solar cells using semiconductor NCs, such as CdTe,[11] PbSe,[12] PbS,[13] and $Cu(In_{1-x}Ga_x)Se_2$,[14] have achieved conversion efficiencies of 2–8% even without high-temperature treatments. One-dimensional (1-D) nanostructures, such as nanorods and nanowires, have also been employed to make light absorbers.[15]

Herein, we report the selective synthesis of CAS nanocrystals including $CuSbS_2$, Cu_3SbS_4, and $Cu_{12}Sb_4S_{13}$ using a solution

Received: April 20, 2015
Published: August 3, 2015

DOI: 10.1021/acs.inorgchem.5b00858
Inorg. Chem. 2015, 54, 7840–7845

process. The $CuSbS_2$, Cu_3SbS_3, Cu_3SbS_4, and $Cu_{12}Sb_4S_{13}$ nanostructures (i.e., nanorods and nanocrystals) have been previously synthesized by hot injection methods.[16−20] In particular, $CuSbS_2$ Cu_3SbS_4, and $Cu_{12}Sb_3S_{13}$ NCs exhibit a stable photoresponse under visible light irradiation when employed in photoelectrochemical cells.[16,19] However, to the best of our knowledge, their properties for thin film solar cells have not yet been reported. In this study, we fabricated CAS NC devices with a heterostructure consisting of ITO-glass/ZnO/CdS/CAS NCs/Au (ITO = indium tin oxide) and studied solar cell performance of these devices. In addition, the different crystal phases were selectively obtained by tuning the ratio of metal precursor to sulfur (or capping agent). Their band structures were also characterized by photoemission yield spectroscopy (PYS) and UV−vis−NIR (NIR = near-IR) spectroscopy to evaluate the applicability of the CAS NCs for solar cell applications.

EXPERIMENTAL SECTION

Chemicals. Copper(II) acetylacetonate (99.99%), antimony(III) acetate (99.99%), triethyloxionium tetrafluoroborate (97.0%), and cadmium sulfate (99.99%) were purchased from Sigma-Aldrich. Sulfur powder and *N*,*N*-dimethylformamide (DMF, 99.5%) were purchased from Kishida Chemicals. Oleylamine (90%) and oleic acid (95%) were purchased from Wako Chemicals. Acetonitrile (99.5%) was purchased from the Tokyo Chemical Industry Co., Ltd.

Synthesis of $CuSbS_2$ Nanocrystals. The $CuSbS_2$ samples were synthesized using a solution process. Typically, Cu(II) acetylacetonate (1 mmol) and Sb(III) acetate (1 mmol) were dissolved in oleylamine (5 mL), and the mixture was heated at 120 °C for 30 min under vacuum. The temperature was increased to 200 °C in an Ar atmosphere, and then oleylamine (3 mL) containing sulfur (2 mmol) was injected into the mixture. The mixture was maintained at 200 °C for 60 min. After completion of the reaction, the product was washed several times using a mixture of hexane and isopropanol. The product was dispersed in toluene for analysis.

Synthesis of Cu_3SbS_4 Nanocrystals. Typically, Cu(II) acetylacetonate (3 mmol) and Sb(III) acetate (1 mmol) were dissolved in oleylamine (3 mL) and heated at 120 °C for 30 min under vacuum conditions. The temperature was increased to 200 °C in an Ar atmosphere, and then oleylamine (3 mL) containing sulfur (4 mmol) was injected into the mixture. The mixture was maintained at 200 °C for 30 min.

Synthesis of $Cu_{12}Sb_4S_{13}$ Nanocrystals. Typically, Cu(II) acetylacetonate (3 mmol) and Sb(III) acetate (1 mmol) were dissolved in oleylamine (3 mL) and heated at 120 °C for 30 min under vacuum conditions. The temperature was increased to 220 °C in an Ar atmosphere, and then oleylamine (3 mL) containing sulfur (5 mmol) was injected into the mixture. The mixture was heated at 220 °C for 30 min.

Post-Treatment for Cu_3SbS_4 Nanocrystal Synthesis. We also synthesized $Cu_{12}Sb_4S_{13}$ NCs by converting Cu_3SbS_4 NCs in a post-treatment process. A hexane solution containing the as-synthesized Cu_3SbS_4 NCs was mixed with an oleylamine solution containing sulfur (3 mmol) in a three-neck flask. The mixture was heated to 120 °C for 30 min under vacuum. The temperature was increased to 230 °C and heated for 30 min. The product was washed several times using a mixture of hexane and isopropanol.

Material Characterization. The synthesized crystals were analyzed by X-ray diffractometry (XRD) using Cu Kα radiation (RINT2100, Rigaku) and transmission electron microscopy (TEM; JEM-2000EX/T, JEOL). The valence-band edge positions were analyzed by PYS in air using a commercial instrument (AC-2, RIKEN KEIKI Co., Ltd). The light absorbance spectra were recorded on a UV−vis−NIR spectrometer (UV-3100, Shimadzu). The elemental compositions of the NCs were determined using inductively coupled plasma atomic emission spectroscopy (ICP-AES; SPS1700 HVR, Seiko Instruments Inc).

Device Fabrication and Testing. Patterned ITO-coated glass substrates (15 Ω/sq) were purchased from the Kintec Company and cleaned with acetone and deionized water under sonication for 5 min prior to use. A ZnO window layer (thickness: 200 nm) was deposited on ITO glass by drop casting using a ZnO NCs ink. The ZnO NCs were synthesized according to a previously reported method.[21] After deposition, the ZnO film was heated to 300 °C for 30 min to remove the capping agents from the ZnO NCs surface. A CdS buffer layer (thickness: 30 nm) was deposited on the resulting ZnO film using a chemical bath deposition method. The glass substrate with the ZnO layer was placed on a hot plate and heated at 90 °C. Then, an aqueous solution containing 0.015 M $CdSO_4$ and 1.5 M thiourea (amount ratio 1:1) was dropped onto the substrate. The pH of the solution was adjusted to 10 by the addition of NH_4OH. The substrate was removed from the hot plate after 3 min and rinsed with deionized water. A CAS absorber layer (thickness: 100−300 nm) was deposited on the CdS layer by spin coating using a toluene dispersion containing CAS NCs. The rotation speed was 2000 rpm, and the NC concentration of the ink was ca. 0.15 mg/mL. The film was subjected to ligand stripping, which is described in the next section. Finally, the film was coated with gold electrodes (thickness: 100 nm) using vacuum thermal evaporation. The solar cell structure consisted of glass/ITO/ZnO/CdS/CAS/Au. The PV response was measured using a Keithly 2400 source meter under light irradiation from a solar simulator (PEC-L15, Peccell Technologies, Inc.) equipped with an AM 1.5 filter (100 mW/cm^2).

Stripping of Oleylamine Ligands from Nanocrystals. The oleylamine ligands were removed from the CAS NC surface with Meerwein's agent ($(C_2H_5)_3OBF_4$) according to a previously described method.[21,22] The spin-coated CAS film was soaked in acetonitrile containing $(C_2H_5)_3OBF_4$ (100 mM, 10 mL) for 5 min. Then, the film was washed with acetonitrile containing DMF (1 M, 10 mL). The treated films were carefully cleaned with hexane. After completion of the reaction, the CAS NCs were no longer soluble in hexane, indicating the elimination of oleylamine from the surface. The absence of surface ligands was confirmed by Fourier transform infrared spectroscopy (FTIR 4100, Jasco).

RESULTS AND DISCUSSION

The morphology of the CAS NCs was studied using TEM. Figure 1 shows representative TEM images of (a) $CuSbS_2$, (b) Cu_3SbS_4, and (c) $Cu_{12}Sb_4S_{13}$ NCs. The $CuSbS_2$ and $Cu_{12}Sb_4S_{13}$ NCs had a rod shape. The rod sizes of the $CuSbS_2$ and $Cu_{12}Sb_4S_{13}$ NCs were ca. 50 nm in diameter and ca. 1 μm in length and ca. 10 nm in diameter and ca. 40 nm in length, respectively. The rod length of the $Cu_{12}Sb_4S_{13}$ NCs was much

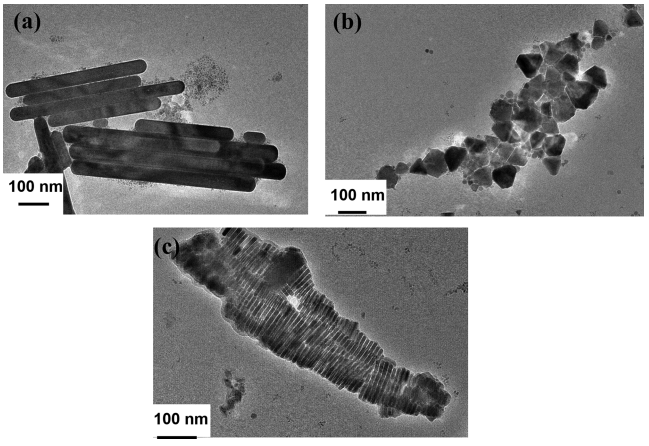

Figure 1. TEM images of the (a) $CuSbS_2$, (b) Cu_3SbS_4, and (c) $Cu_{12}Sb_4S_{13}$ NCs.

DOI: 10.1021/acs.inorgchem.5b00858
Inorg. Chem. 2015, 54, 7840−7845

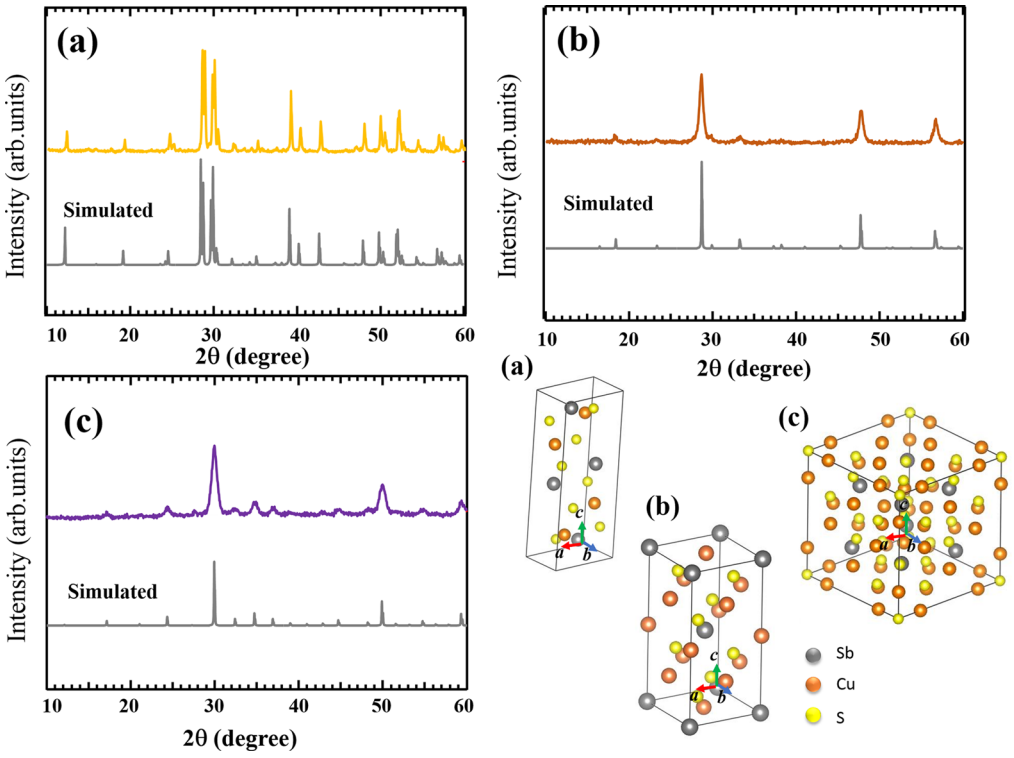

Figure 2. XRD patterns of the (a) $CuSbS_2$, (b) Cu_3SbS_4, and (c) $Cu_{12}Sb_4S_{13}$ NCs along with their crystal structures.

shorter than that of $CuSbS_2$ NCs. In addition, the Cu_3SbS_4 NCs had an irregular shape with a diameter of ca. 80 nm.

Next, the crystallite phase and phase purity of the samples was studied using XRD. Figure 2a–c shows the XRD patterns of the as-synthesized $CuSbS_2$, Cu_3SbS_4, and $Cu_{12}Sb_4S_{13}$ NCs. Their patterns were in good agreement with the simulated patterns of chalcostibite (space group: *Pnma*, a = 6.018 Å, b = 3.7958 Å, c = 14.498 Å, and $\alpha = \beta = \gamma = 90°$), fematinite (space group: $I\bar{4}2m$; $a = b$ = 5.2855 Å, c = 10.7483 Å and $\alpha = \beta = \gamma = 90°$), and tetrahedrite (space group: $I\bar{4}3m$; $a = b = c$ = 10.323 Å and $\alpha = \beta = \gamma = 90°$). These crystal structures are also shown in Figure 2. The XRD patterns indicate the good crystallinity and phase purity of the synthesized CAS NCs. The elemental compositions of $CuSbS_2$, Cu_3SbS_4, and $Cu_{12}Sb_4S_{13}$ were estimated to be $Cu_{1.0}Sb_{1.0}S_{1.8}$, $Cu_{2.9}Sb_{1.0}S_{3.9}$, and $Cu_{11.6}Sb_{4.0}S_{14.4}$, respectively, from ICP-AES measurements. $CuSbS_2$ and Cu_3SbS_4 had slightly sulfur-deficient compositions compared to their stoichiometric compositions, and $Cu_{12}Sb_4S_{13}$ contained excess sulfur. On the basis of these results, this method selectively produced CAS with different compositions and crystal structures. In contrast, heating the reaction system containing all of the precursors to 200–220 °C without injecting sulfur at high temperatures generated a mixture of Cu_3SbS_4 and $Cu_{12}Sb_4S_{13}$ NCs. Therefore, the phase stability of $CuSbS_2$, Cu_3SbS_4, and $Cu_{12}Sb_4S_{13}$ NCs was strongly affected by the synthesis conditions including the reaction temperature and precursor ratio.

Because the CAS systems have multiple phases, phase transformations between the respective phases may be possible under controlled conditions. Notably, Cu_3SbS_4 and $Cu_{12}Sb_4S_{13}$ were synthesized using the same metal precursor ratio and slightly different sulfur amounts at different temperatures (220 and 200 °C). Therefore, we attempted phase conversion of Cu_3SbS_4 to $Cu_{12}Sb_4S_{13}$ using a post-treatment process. Figure 3 shows the XRD patterns (a) before and (b) after post-

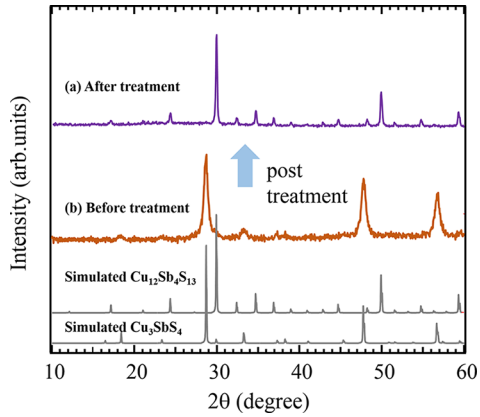

Figure 3. XRD patterns (a) after and (b) before post-treatment of the as-synthesized Cu_3SbS_4 NCs in a sulfur-containing oleylamine solution at 230 °C.

treatment for the as-synthesized Cu_3SbS_4 NCs. The XRD pattern of the NCs after treatment confirmed that the phase transformation from famanitite (Cu_3SbS_4) to tetrahedrite ($Cu_{12}Sb_4S_{13}$) occurred by reheating the Cu_3SbS_4 NCs. The formation of tetrahedrite was most likely due to the loss of sulfur from the crystal lattice, leading to a change in the crystal structure. For charge neutrality, the valence changes from Cu(I) to Cu(II) and Sb(V) to Sb(III) also occurred, producing tetrahedrite by post-treatment as shown below.

$$Cu_3^{(I)}Sb^{(V)}S_4 \rightarrow Cu_{10}^{(I)}Cu_2^{(II)}Sb_4^{(III)}S_{13}$$

Embden et al. also reported the crystal structure change of CAS NCs deposited on a substrate where heat treatment in a sulfur atmosphere at 350 °C converted $Cu_{12}Sb_4S_{13}$ to Cu_3SbS_4.[19] The obtained results coupled with the reported ones suggest the possibility of reversible control of the crystal

DOI: 10.1021/acs.inorgchem.5b00858
Inorg. Chem. 2015, 54, 7840–7845

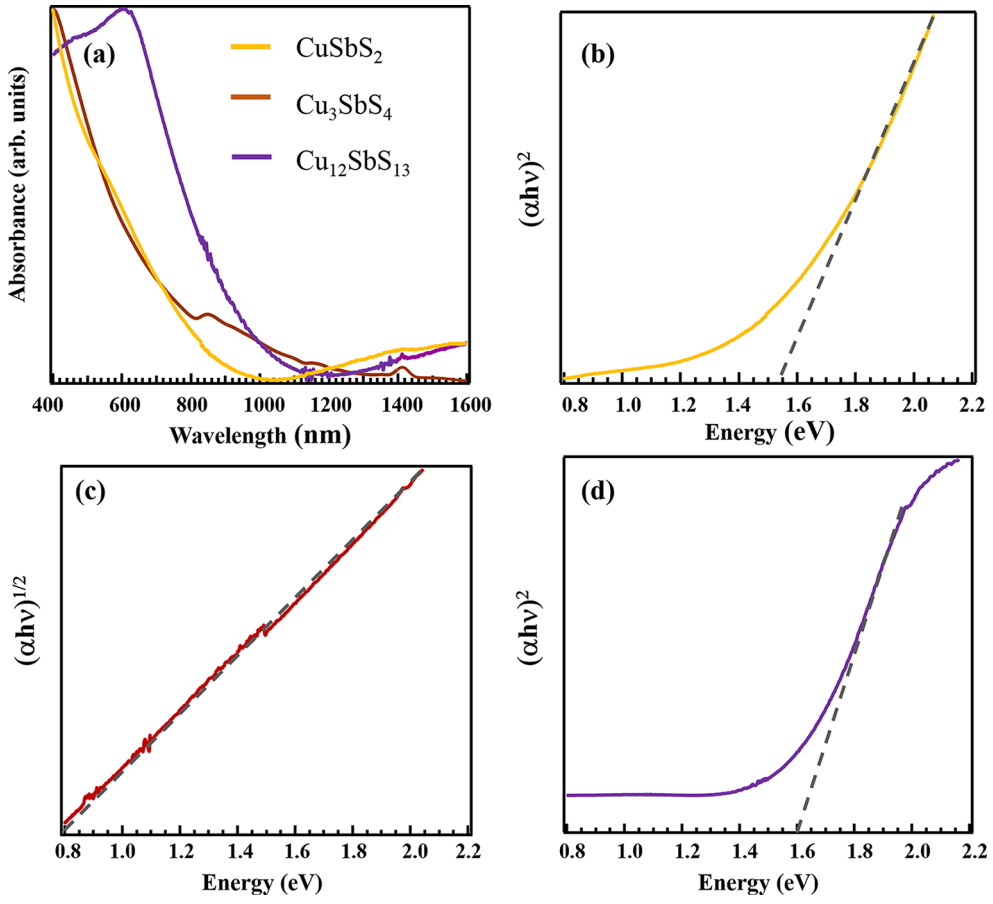

Figure 4. (a) UV−vis−NIR spectra of CAS NCs along with their corresponding $(\alpha h\nu)^n$ (n = 2 or 1/2) as a function of photon energy plots for the (b) $CuSbS_2$, (c) Cu_3SbS_4, and (d) $Cu_{12}Sb_4S_{13}$ NCs.

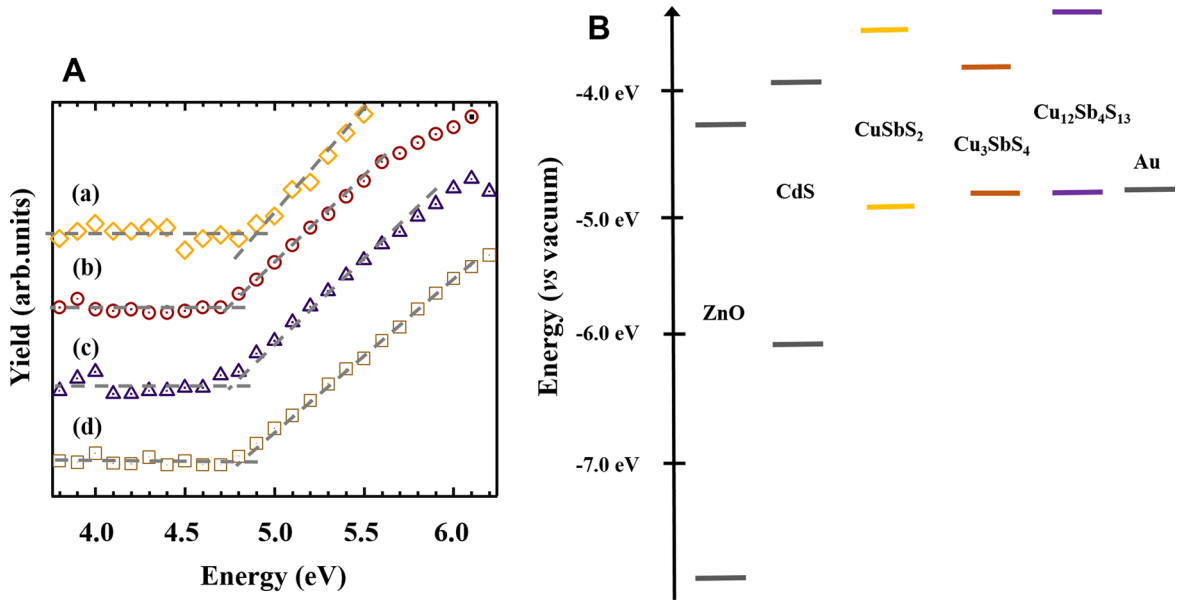

Figure 5. (A) PYS spectra of the (a) $CuSbS_2$, (b) Cu_3SbS_4, and (c) $Cu_{12}Sb_4S_{13}$ NCs and (d) a gold electrode. (B) Estimated band energy diagrams for the $CuSbS_2$, $Cu_{12}Sb_4S_{13}$, and Cu_3SbS_4 NCs along with those for Au, ZnO, and CdS.

structure and the resulting physical properties, such as the optical bandgap, electron conductivity, and magnetic susceptibility, in the CAS NC system.

Figure 4 shows the UV−vis−NIR absorption spectra of the CAS NCs in toluene along with the corresponding Tauc plots ($(\alpha h\nu)^n$ vs $h\nu$, n = 2 or 1/2). The $CuSbS_2$ NCs exhibited an absorption onset at ∼1150 nm, and its band gap was calculated to be ca. 1.5 eV from the Tauc plot, which was nearly the same as the reported value.[16] The absorption edges of Cu_3SbS_4 and $Cu_{12}Sb_4S_{13}$ were located at ∼1500 nm (band gap: ca. 0.8 eV)

DOI: 10.1021/acs.inorgchem.5b00858
Inorg. Chem. 2015, 54, 7840−7845

and 1050 nm (band gap: 1.6 eV), respectively. These values are also in good agreement with those previously reported.[19] The linear fitting of $(\alpha h\nu)^2$ as a function of the photon energy at n = 2 was possible for the $CuSbS_2$ and $Cu_{12}Sb_4S_{13}$ NCs, suggesting that they are direct band gap semiconductors. Kumar et al. calculated the electronic band structure of $CuSbS_2$ using density functional theory calculations and reported that $CuSbS_2$ is an indirect material.[7] However, their results did not agree with the experimental results that indicated that $CuSbS_2$ was a direct material.[23] Our results also indicated that $CuSbS_2$ NCs had a direct band gap, which agrees with the reported results for the $CuSbS_2$ nanobricks and nanoplates.[16,18] However, previous studies have reported that $CuSbS_2$ NC is an indirect band gap material.[17,24] A possible reason for the discrepancies between the theoretical and experimental band gaps is the presence/absence of impurities or defects in the $CuSbS_2$ NCs, as suggested by Kumar et al.[7] In contrast to the $CuSbS_2$ and $Cu_{12}Sb_4S_{13}$ NCs, the Cu_3SbS_4 NCs exhibited a behavior consistent with indirect band gap semiconductors (n = 1/2). In addition, the $CuSbS_2$ and $Cu_{12}Sb_4S_{13}$ NCs exhibited a gradual increase in absorbance in the NIR wavelength region. The NIR absorption has been previously reported in the CAS system.[19] This absorption was due to midband gap states but not due to localized surface plasmon resonance (LSPR) states, which have been observed for copper-deficient sulfides, such as $Cu_{2-x}S_2$ and $Cu_{1-x}InS_2$.[25,26]

To estimate the band structures of these CAS NCs, their valence-band edge positions were measured by PYS, as shown in Figure 5A. The valence-band edge position was determined from the threshold of the photoemission (the intersection of the baseline with the straight line in the figure). The conduction-band edge positions of the CAS NCs were estimated from the valence-band edge positions and their band gaps that were determined using UV−vis−NIR spectroscopy. The work function of gold was determined to be 4.8 eV and is in good agreement with the reported value, suggesting the validity of these measurements. The estimated band energy diagrams of the CAS NCs are shown in Figure 5B, which shows a clear difference in the electronic structure of the NCs with different compositions and crystal structures.

Next, the PV devices with a heterostructure consisting of glass/ITO/CAS NCs/CdS/Al were studied. The NC surface was subjected to ligand stripping using an alkylating agent ($(C_2H_5)_3OBF_4$) to remove the surface insulating layers. Figure 6 shows the typical current−voltage (I−V) curves for devices using CAS NC particulate films. The devices exhibited a diode-like behavior, and the current increased as the voltage increased in a forward direction. This result indicates the successful formation of a p−n heterojunction between the CAS film (p-type) and the CdS film (n-type), which indicates the potential applicability of CAS NCs for use in electronic devices. According to the band energy diagram, the mismatch of the conduction-band edges between the CAS NCs and CdS is not significant, which may allow for charge separation at the junction interface even though the electronic structure of this junction remains unclear due to the absence of information on the Fermi levels. It is important to note that for the I−V curves, the currents also flowed in the reverse direction, suggesting poor junction quality. In addition, the device exhibited no PV response under simulated sunlight, which may indicate that the light did not reach the junction interface when irradiated from the CAS side (ITO side) due to the high light absorption coefficient of the CAS materials. Therefore, we revised the

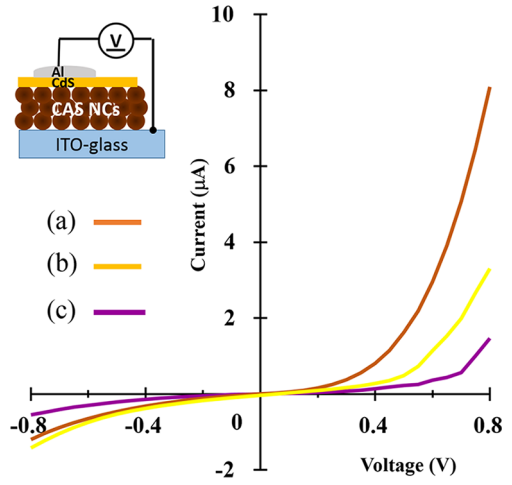

Figure 6. Current−voltage (I−V) curves for the (a) $CuSbS_2$, (b) Cu_3SbS_4, and (c) $Cu_{12}Sb_4S_{13}$ NC films coupled with CdS layers.

device structure and fabricated PV devices with a structure consisting of glass/ITO/ZnO/CdS/CAS/Au.

Figure 7 shows the representative I−V characteristics of the $CuSbS_2$ NC device with the modified structure. The device

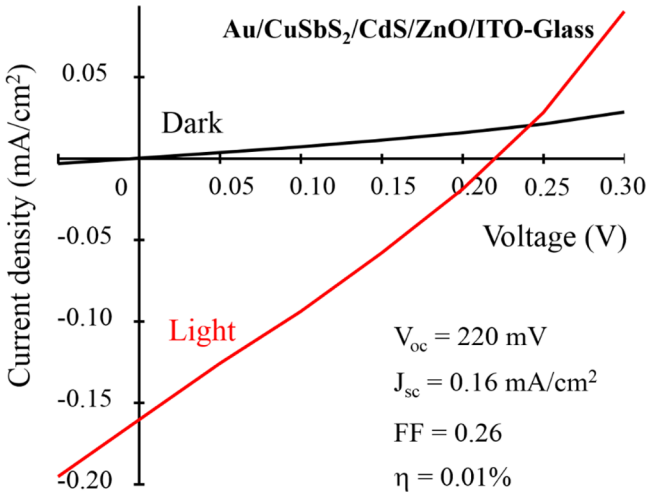

Figure 7. Current−voltage (I−V) curves for the $CuSbS_2$ device with a structure consisting of ITO/ZnO/CdS/$CuSbS_2$/Au under simulated sunlight and in the dark.

exhibited a clear PV response under simulated sunlight (100 mW/cm^2). The absorption onsets of the ZnO and CdS films were observed at ∼400 and 500 nm, respectively.[21] Therefore, most of the visible light reached the p−n junction interface between the CdS and CAS NC layers and generated charge carriers at the interface upon irradiation. As shown in Figure 5, the conduction-band edge position of the $CuSbS_2$ NC is more negative than that of CdS, and the valence-band edge position of CdS is more positive than that of $CuSbS_2$ NC. Therefore, the photogenerated electrons and holes at the p−n junction interface move to the CdS and $CuSbS_2$ NC layers, respectively. This charge carrier separation at the junction produced a PV response in the $CuSbS_2$ NC-based device. $CuSbS_2$ nanobricks exhibit a p-type behavior, as revealed by photoelectrochemical measurements.[16] The Cu_3SbS_4 and $Cu_{12}Sb_3S_{13}$ NCs also exhibited a p-type photocurrent response under visible light irradiation.[19] In addition, the $CuSbS_2$ films prepared using a

DOI: 10.1021/acs.inorgchem.5b00858
Inorg. Chem. 2015, 54, 7840−7845

solution process have a p-type conductivity based on Hall measurements.[10] Therefore, the Cu−Sb−S systems are intrinsically p-type materials. We confirmed that no current rectification behavior was observed without a $CuSbS_2$ NC layer in our solar cell. Therefore, the synthesized $CuSbS_2$ NCs are p-type materials that can promote charge separation when combined with an n-type material.

The power conversion efficiency (η) was calculated to be 0.01% with V_{oc} of 306 mV, J_{sc} of 0.17 mA/cm^2, and fill factor (FF) of 0.28. The obtained efficiency was very low compared to the reported values for other NC-based devices. Even using a thick dense $CuSbS_2$ layer fabricated with a high-temperature treatment, the reported efficiency remained low (η = 0.5%).[10] However, a PV response was observed in the present case even without heat treatment. Therefore, these results hold a promise for potential applications of the $CuSbS_2$ NCs in solar cells. In contrast, Cu_3SbS_4 and $Cu_{12}Sb_4S_{13}$ NC devices exhibited no clear PV response. The reason for this result remains unclear. The presence of surface trap sites or impurity phases that cannot be detected by XRD is possible. Careful control of the absorber layer thickness, surface conditions, and device structure may be necessary to observe a PV response from Cu_3SbS_4 and $Cu_{12}Sb_4S_{13}$ NC devices.

CONCLUSIONS

Copper−antimony-sulfide (CAS) nanocrystals including $CuSbS_2$, Cu_3SbS_4, and $Cu_{12}Sb_4S_{13}$ were synthesized using a solution-phase synthetic approach. The crystal phase control was achieved by changing the reaction temperature and starting precursor ratios. The crystal morphologies were dependent on the crystal phase. $CuSbS_2$ and $Cu_{12}Sb_4S_{13}$ were rodlike crystals, and Cu_3SbS_4 was an irregular crystal. The results from photoemission yield measurements and UV−vis−NIR spectroscopy revealed differences in the electronic structures of the three phases. Devices that coupled of the CAS particulate films with dense CdS layers showed a diodelike behavior, suggesting the formation of a p−n heterojunction between CAS and CdS. Devices based on the ITO/ZnO/CdS/$CuSbS_2$/Au structure exhibited a PV response with a power conversion efficiency of 0.01% under simulated sunlight. However, devices prepared with Cu_3SbS_4 and $Cu_{12}Sb_4S_{13}$ exhibited no PV response. Although the obtained efficiency was very low for practical applications, improving the film quality by sintering and optimizing the thickness would further boost the performance.

The present device structure is suitable to test the potential of the new absorber materials. Wet chemical methods allow for easier fabrication of a thin film than vacuum methods in terms of cost and time. Indeed, we observed distinct PV responses from Cu_2ZnSnS_4 and $CuInS_2$ NCs using the same structure.[21] Therefore, our methodology using a nanocrystal ink for thin film fabrication would offer an efficient and easy approach for screening various materials for new solar cell absorbers.

AUTHOR INFORMATION

Corresponding Author

*E-mail: tetsuya@kumamoto-u.ac.jp.

Notes

The authors declare no competing financial interest.

ACKNOWLEDGMENTS

This work was supported by research grants from the Hosokawa Powder Technology Foundation.

REFERENCES

(1) Britt, J.; Ferekides, C. *Appl. Phys. Lett.* **1993**, *62*, 2851−2852.
(2) Green, M. A.; Emery, K.; Hishikawa, Y.; Warta, W. *Prog. Photovoltaics* **2010**, *18*, 346−352.
(3) Katagiri, H.; Sasaguchi, N.; Hando, S.; Hoshino, S.; Ohashi, J.; Yokota, T. *Sol. Energy Mater. Sol. Cells* **1997**, *49*, 407−414.
(4) Cao, Y.; Denny, M. S., Jr; Caspar, J. V.; Farneth, W. E.; Guo, Q.; Ionkin, A. S.; Johnson, L. K.; Lu, M.; Malajovich, I.; Radu, D.; Rosenfeld, H. D.; Choudhury, K. R.; Wu, W. *J. Am. Chem. Soc.* **2012**, *134*, 15644−15647.
(5) Puthussery, J.; Seefeld, S.; Berry, N.; Gibbs, M.; Law, M. *J. Am. Chem. Soc.* **2011**, *133*, 716−719.
(6) Bashkirov, S. A.; Gremenok, V. F.; Ivanov, V. A.; Lazenka, V. V.; Bente, K. *Thin Solid Films* **2012**, *520*, 5807−5810.
(7) Kumar, M.; Persson, C. *J. Renewable Sustainable Energy* **2013**, *5*, 031616−031621.
(8) Dufton, J. T. R.; Walsh, A.; Panchmatia, P. M.; Peter, L. M.; Colombara, D.; Islam, M. S. *Phys. Chem. Chem. Phys.* **2012**, *14*, 7229−7233.
(9) Rodriguez-Lazcano, Y.; Nair, M. T. S.; Nair, P. K. *J. Electrochem. Soc.* **2005**, *152*, G635−G638.
(10) Yang, B.; Wang, L.; Han, J.; Zhou, Y.; Song, H.; Chen, S.; Zhong, J.; Lv, L.; Niu, D.; Tang, J. *Chem. Mater.* **2014**, *26*, 3135−3143.
(11) Gur, I.; Fromer, N. A.; Geier, M. L.; Alivisatos, A. P. *Science* **2005**, *310*, 462−465.
(12) Luther, J. M.; Law, M.; Beard, M. C.; Song, Q.; Reese, M. O.; Ellingson, R. J.; Nozik, A. J. *Nano Lett.* **2008**, *8*, 3488−3492.
(13) Maraghechi, P.; Labelle, A. J.; Kirmani, A. R.; Lan, X.; Adachi, M. M.; Thon, S. M.; Hoogland, S.; Lee, A.; Ning, Z.; Fischer, A.; Amassian, A.; Sargent, E. H. *ACS Nano* **2013**, *7*, 6111−6116.
(14) Lee, J. H.; Chang, J.; Cha, J.-H.; Lee, Y.; Han, J. E.; Jung, D.-Y.; Choi, E. C.; Hong, B. *Eur. J. Inorg. Chem.* **2011**, *2011*, 647−651.
(15) Yu, K.; Chen, J. *Nanoscale Res. Lett.* **2009**, *4*, 1−10.
(16) Yan, C.; Su, Z.; Gu, E.; Cao, T.; Yang, J.; Liu, J.; Liu, F.; Lai, Y.; Li, J.; Liu, Y. *RSC Adv.* **2012**, *2*, 10481−10484.
(17) Xu, D.; Shen, S.; Zhang, Y.; Gu, H.; Wang, Q. *Inorg. Chem.* **2013**, *52*, 12958−12962.
(18) Ramasamy, K.; Sims, H.; Butler, W. H.; Gupta, A. *J. Am. Chem. Soc.* **2014**, *136*, 1587−1598.
(19) Van Embden, J.; Latham, K.; Duffy, N. W.; Tachibana, Y. *J. Am. Chem. Soc.* **2013**, *135*, 11562−11571.
(20) Van Embden, J.; Tachibana, Y. *J. Mater. Chem.* **2012**, *22*, 11466−11469.
(21) Suehiro, S.; Horita, K.; Yuasa, M.; Tanaka, T.; Fujita, K.; Shimanoe, K.; Kida, T.; Kumamoto, K. *J. Phys. Chem. C* **2014**, *118*, 804−810.
(22) Rosen, E. L.; Buonsanti, R.; Llordes, A.; Sawvel, A. M.; Milliron, D. J.; Helms, B. A. *Angew. Chem., Int. Ed.* **2012**, *51*, 684−689.
(23) Rabhi, A.; Kanzari, M.; Rezig, B. *Thin Solid Films* **2009**, *517*, 2477−2480.
(24) Ramasamy, K.; Sims, H.; Butler, W. H.; Gupta. *Chem. Mater.* **2014**, *26*, 2891−2899.
(25) Luther, J. M.; Jain, P. K.; Ewers, T.; Alivisatos, A. P. *Nat. Mater.* **2011**, *10*, 361−366.
(26) Niezgoda, J. S.; Yap, E.; Keene, J. D.; McBride, J. R.; Rosenthal, S. J. *Nano Lett.* **2014**, *14*, 3262−3269.

DOI: 10.1021/acs.inorgchem.5b00858
Inorg. Chem. 2015, 54, 7840−7845